THE JOURNAL OF PHYSICAL CHEMISTRY C

Article

pubs.acs.org/JPCC

Active, Simple Iridium–Copper Hydrous Oxide Electrocatalysts for Water Oxidation

Chao Wang,[†] Reza B. Moghaddam,[†,‡] and Steven H. Bergens*[,†]

[†]Department of Chemistry, University of Alberta, 11227 Saskatchewan Drive, Edmonton, Alberta T6G 2G2, Canada

[‡]Department of Electrical and Computer Engineering, University of Alberta, 9211 116 Street NW, Edmonton, Alberta T6G 2V4, Canada

Supporting Information

ABSTRACT: A series of $Ir_{1-x}Cu_x$ (x = 0–0.5) hydrous oxide nanoparticles (HO-np) were prepared simply by stirring solutions of $IrCl_3$ hydrate and $CuCl_2$ hydrate in aqueous KOH under air. Their water oxidation activities were measured in 0.1 M $HClO_4$. The $Ir_{0.89}Cu_{0.11}$ HO-np was the most active catalyst in the series with mass (Ir) – normalized activity = 142 A g_{Ir}^{-1} and electrochemically accessible Ir sites normalized activity >180 A $mmol_{Ir}^{-1}$ (both at 250 mV overpotential). The $Ir_{0.89}Cu_{0.11}$ HO-nps were stable for 24 h galvanostatic oxidations at 1 mA $cm^{-2}_{geometric}$, with only 280 mV overpotential. The average diameter of the $Ir_{0.89}Cu_{0.11}$ HO-nps was ~1.30 nm. XPS results suggested that doping with Cu^{2+} reduces the overall charge in the lattice, resulting in higher electron density at Ir than in pure Ir HO-np. Preliminary mechanistic investigations showed that the activity enhancement by Cu is not only a surface area effect, and the presence of Cu does not appear to significantly alter the mechanism of the water oxidation reaction.

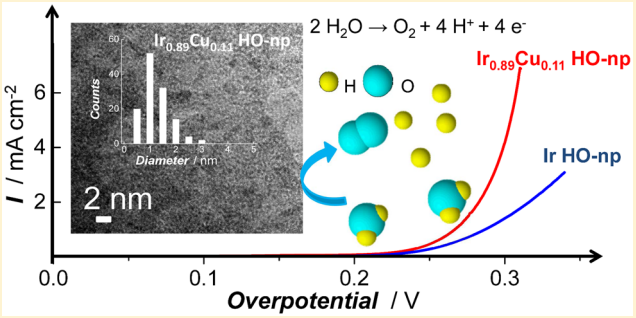

INTRODUCTION

The production of hydrogen by water electrolysis is a promising method to store energy from renewable sources such as wind and solar.[1−5] Proton exchange membranes (PEM's) are ideally suited for water electrolyzers because they provide low ohmic losses, large partial load ranges, and high current densities.[6−8] The anode catalysts of PEM electrolyzers must operate at oxidizing potentials for long periods of time under acidic conditions at moderate to high temperatures.[7,9] Non-noble catalysts mostly dissolve under these conditions, and oxides of noble metals are presently required in the most stable catalysts for the water oxidation reaction (WOR) in acid.[6−8] Further, the kinetics of the 4-electron water oxidation reaction are slow, and require high catalyst loadings in electrolyzer anodes to produce practical current densities at moderate overpotentials.[10] Because of these challenges, developing stable and active at low loading WOR electrocatalysts is the major barrier to the widespread utilization of PEM electrolyzers.

Typically, catalysts containing Ru are the most active for the WOR in acid, but RuO_x undergoes severe dissolution during prolonged operation.[11,12] Pure Ir hydrous oxides have promising activity and good stability toward the WOR in acid, but the scarcity of Ir restricts the widespread application of electrolyzers.[6,13−17] A high priority in WOR research is to increase the activity of Ir catalysts while maintaining their stability. It was shown that combining Ir with a 3d-transition metal like Ni or Co reduces the Ir content and increases the activity of WOR catalysts.[16,18−22] Also, the structures of Ir-containing WOR catalysts have been modified to increase their activities. For example, Strasser et al. showed that nanoparticles consisting of Ir–Ni metallic cores and largely IrO_x shells catalyzed the WOR with mass current density = 40 A g_{Ir}^{-1} at 0.25 V overpotential in 0.05 M H_2SO_4 (loading 10.2 μg_{Ir} cm^{-2}).[16] The Strasser group subsequently reported that core–shell $IrNiO_x$ nanoparticles supported on *meso*-ATO and annealed at 180 °C operated with mass current density = 90 A g_{Ir}^{-1} at 0.28 V overpotential in 0.05 M H_2SO_4. This activity is 2.5 times higher than IrO_x nanoparticles prepared in the same manner (loading 10.2 μg_{Ir} cm^{-2}).[22] We recently reported that a range of $IrNi_yO_x$ hydrous oxide nanoparticles (HO-np) are prepared by stirring Ir- and Ni-chlorides in aqueous base under air. The resulting $IrNi_{0.125}$ ($Ir_{0.89}Ni_{0.11}$) HO-np catalyze the WOR at >140 A g_{Ir}^{-1} at 0.25 V overpotential with good stability in 0.1 M H_2SO_4 (loading 17.3 μg_{Ir} cm^{-2}).[18] Despite its high abundance, and widespread use as an electrocatalyst, we are aware of only two reports of the incorporation of Cu into IrO_x catalysts for WOR in acid. Zou et al. synthesized Cu–Ir nanocages by a galvanic replacement method, and reported 73 mA mg^{-1} mass activity for $Cu_{1.11}Ir$ nanocages at 0.28 V overpotential in 0.05 M H_2SO_4 (loading 143 μg cm^{-2}).[20] Sun et al. obtained 50 A g^{-1} mass activity at 0.35 V overpotential in 0.1

Received: December 2, 2016
Revised: January 18, 2017
Published: February 16, 2017

Downloaded via UNIV OF ALBERTA on July 4, 2018 at 16:57:26 (UTC).
See https://pubs.acs.org/sharingguidelines for options on how to legitimately share published articles.

© 2017 American Chemical Society

DOI: 10.1021/acs.jpcc.6b12164
J. Phys. Chem. C 2017, 121, 5480−5486

M $HClO_4$ (loading 200 $\mu g\ cm^{-2}$) with $Cu_{0.3}Ir_{0.7}$ oxides that were prepared by a hydrothermal method.[19]

In this study, we prepared a series of $Ir_{1-x}Cu_x$ HO-np by stirring $IrCl_3$ and $CuCl_2$ hydrates in aqueous KOH under air.[18] The HO-np were characterized and they are extremely active toward the WOR in acid.

EXPERIMENTAL SECTION

Perchloric acid (Aldrich; 70%, 99.999% trace metal basis), sulfuric acid (Caledon), hydrogen peroxide (Fischer Scientific; 30%), L-ascorbic acid (Fisher; reagent grade), potassium hydroxide (Aldrich; semiconductor grade, 99.99%), carbon fiber paper (ElectroChem, Inc.), iridium chloride trihydrate (A.B. Mackay Chemicals), cupric chloride dihydrate (BDH Chemicals Ltd. Poole England; 98%), *tert*-butanol (Aldrich; > 99%), and Nafion (5 wt %, ElectroChem, Inc.) were used as received. Triply distilled water was used throughout the experiments. All the glassware was cleaned with Piranha solution (5:1 volume ratio of sulfuric acid to 30% hydrogen peroxide) before use.

Colloidal suspensions of the $Ir_{1-x}Cu_x$ HO-np were prepared by adding 0.8 M KOH to 20 mL solutions of $IrCl_3{\cdot}3H_2O$ and $CuCl_2{\cdot}2H_2O$. The amount of Ir was kept constant, with $CuCl_2{\cdot}2H_2O$ added to give the desired fraction x. The amount of KOH added was ~10 times the moles of Ir + Cu. Table 1 shows the amounts used. The molar ratios of the precursor mixtures were $Ir_{0.66}Cu_{0.34}$, $Ir_{0.80}Cu_{0.20}$, $Ir_{0.86}Cu_{0.14}$, $Ir_{0.89}Cu_{0.11}$, and $Ir_{0.92}Cu_{0.08}$. The mixtures were stirred under air for 3 days after addition of the KOH solution. The solutions could be stored in glass vials under air at room temperature for at least 2 months without losing activity.

Table 1. Amounts of Reagents in the Syntheses of $Ir_{1-x}Cu_x$ HO-np (x = 0−0.34)

Ir/Cu ratio	$IrCl_3{\cdot}3H_2O$/g	$CuCl_2{\cdot}2H_2O$/g	added KOH (0.8 M)/mL
Ir	0.0704	0	2.5
$Ir_{0.92}Cu_{0.08}$	0.0706	0.0029	2.7
$Ir_{0.89}Cu_{0.11}$	0.0704	0.0043	2.8
$Ir_{0.86}Cu_{0.14}$	0.0703	0.0057	2.9
$Ir_{0.80}Cu_{0.20}$	0.0705	0.0086	3.1
$Ir_{0.66}Cu_{0.34}$	0.0704	0.0171	3.8

The $Ir_{1-x}Cu_x$ HO-np suspensions were diluted by a factor of 5 with water that contained the appropriate amounts of Nafion to give a final 1% *wt.* Nafion per total mass of Ir + Cu, calculated from the amounts in Table 1. Using a micropipet and graded microtips, 10 μL of the Ir HO-np/Nafion suspension (sonicated for 2 min) was drop coated onto ~1 cm^2 surface of a carbon fiber paper (CF; 1 × 3 cm^2, measured using a ruler) electrode to deposit 3.4 μg Ir onto the electrode. The ink was dried over 20 min at 60 °C then left at room temperature for 20 min. For $Ir_{1-x}Cu_x$ HO-np/Nafion suspensions, the amount of ink was adjusted to deposit 3.4 μg of Ir. The actual amount of metal deposited was determined by dissolution in 1 M $HClO_4$ in the presence of ~1 mg ascorbic acid, followed by inductively coupled plasma−mass spectrometry (ICP-MS) analysis. The theoretical mass based upon the volume of suspension was ~96% that of value measured by ICP-MS value (Table S1). For the galvanostatic test, a 5 times higher amount of ink was used to deposit 17 μg of Ir on the electrode.

An equal volume of *tert*-butanol was added to the HO-np suspensions to precipitate the catalysts. After agitation for 10 min, the suspension was allowed to settle for 30 min before centrifugation at 4500 rpm for 20 min. The supernatant was decanted, and the remaining precipitate was washed twice by mixing with 1:1 volume *tert*-butanol:H_2O (15 mL), centrifuging at 4500 rpm for 20 min, and then decanting the supernatant. The black precipitates were dried in air at room temperature and used directly for XRD, and they were dispersed by sonification for 10 min in water prior to XPS and HRTEM analysis. A control experiment on the washed $Ir_{0.89}Cu_{0.11}$ HO-np showed that this washing procedure does not change the water oxidation activity of the catalyst (Figure S8).

The electrochemical experiments were performed at room temperature in 0.1 M $HClO_4$ solution, with a Solartron SI 1287 Electrochemical Interface controlled by CorrWare for Windows Version 2−3d software. The reference electrode was a saturated calomel electrode (SCE; Fisher Scientific). The potential of the SCE was calibrated against a Pt electrode under saturated H_2 in 0.1 M $HClO_4$ solution (Figure S5). All potentials in this paper are reported versus RHE. A graphite rod was used as the counter electrode. Uncompensated resistance was measured by AC impedance (8 Ω) and corrected for.

The X-ray photoelectron spectroscopy (XPS) measurements were performed on a Kratos Axis 165 instrument. Inductively coupled plasma−mass spectrometry (ICP-MS) analyses were

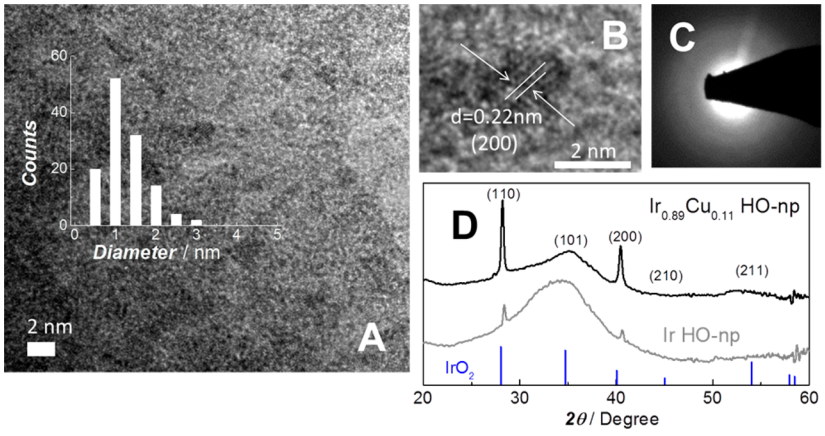

Figure 1. (A and B) HRTEM images of $Ir_{0.89}Cu_{0.11}$ HO-np. (C) Selected area electron diffraction pattern of the $Ir_{0.89}Cu_{0.11}$ HO-np. (D) Powder X-ray diffraction on $Ir_{0.89}Cu_{0.11}$and Ir HO-np.

DOI: 10.1021/acs.jpcc.6b12164
J. Phys. Chem. C 2017, 121, 5480−5486

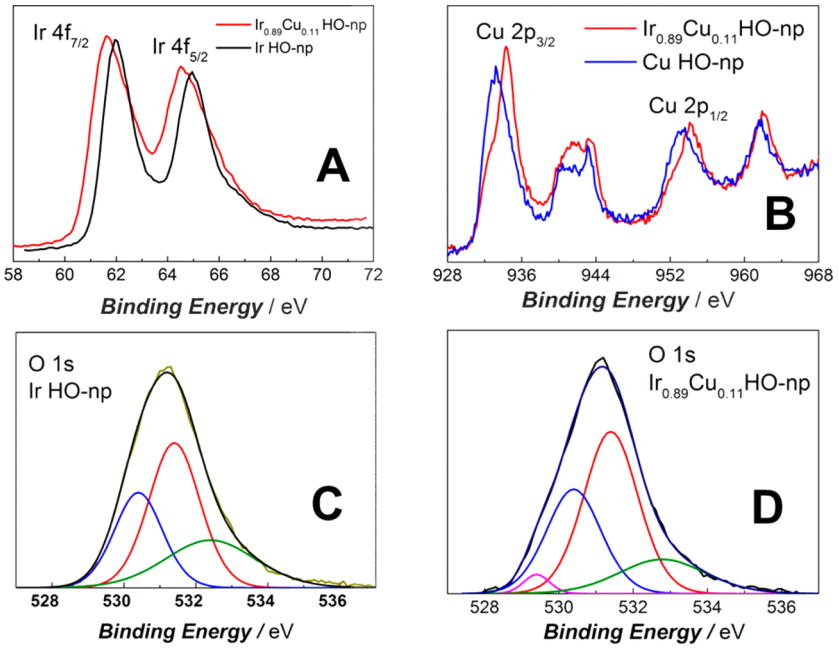

Figure 2. XPS spectra of the $Ir_{0.89}Cu_{0.11}$, Ir and Cu HO-np, Ir 4f region (A), Cu 2p region (B), and O 1s region (C and D).

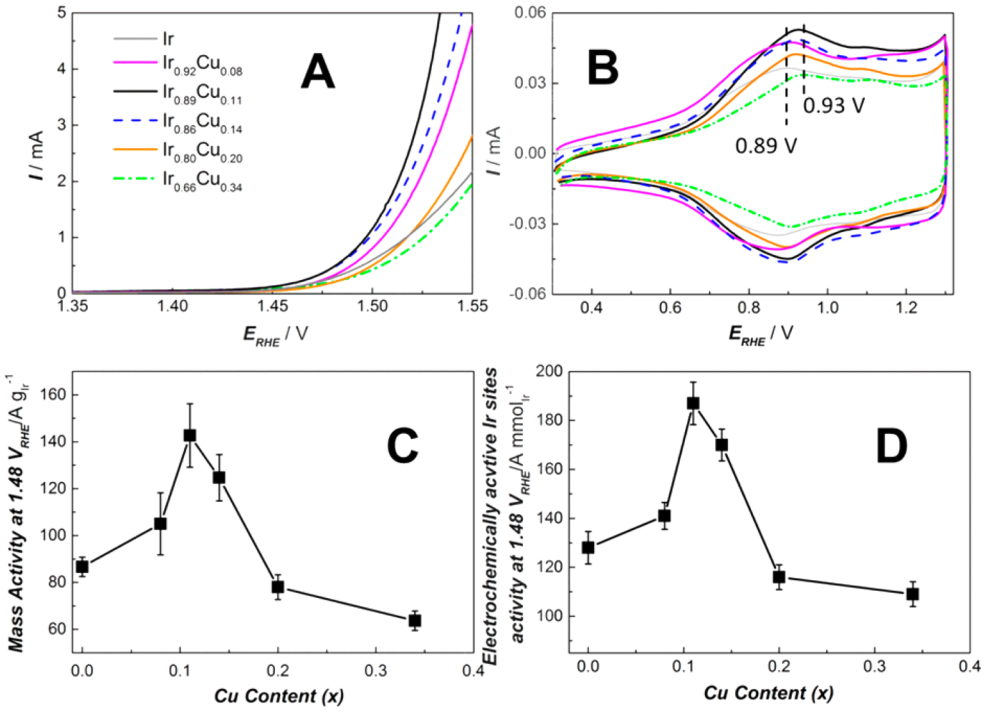

Figure 3. (A) Voltammetric (10 mV s^{-1}) water oxidation by $Ir_{1-x}Cu_x$ HO-np (x = 0–0.5) in 0.1 M $HClO_4$. (B) Cyclic voltammograms (50 mV s^{-1}) of $Ir_{1-x}Cu_x$ HO-np in 0.1 M $HClO_4$. (C and D) Mass and active Ir sites normalized activity at 1.48 V_{RHE}. Mass loading of Ir = 3.4 μg_{Ir} cm^{-2} for all electrodes.

performed with PerkinElmer Elan 6000. High resolution transmission electron microscopy (HRTEM) images were acquired using a Titan 80–300 LB high resolution transmission microscope. Powder X-ray diffraction (XRD) patterns were measured with an X'Pert Pro MPD diffractometer (PANalitical, Netherlands) equipped with a curved position-sensitive detector (CPS 120) and a Cu Kα_1 radiation source at 40 kV and 20 mA ($l_{1/2}$ = 1.54060/1.54439 Å).

RESULTS AND DISCUSSION

As stated previously, a series of $Ir_{1-x}Cu_x$ HO-np were prepared by reacting $IrCl_3$ hydrate and $CuCl_2$ hydrate with aqueous KOH under air. Parts A and B of Figure 1 show the HRTEM images and the size-distribution histogram of the isolated $Ir_{0.89}Cu_{0.11}$ HO-np. This catalyst is the most active water oxidation catalyst in the series (*vide infra*). The sample consists of a mixture of small, crystalline nanoparticles. The average diameter was ~1.30 nm, which is similar to the Ir and $IrNi_{0.125}$

DOI: 10.1021/acs.jpcc.6b12164
J. Phys. Chem. C 2017, 121, 5480–5486

Table 2. Key Electrochemistry Parameters of the $Ir_{1-x}Cu_x$ HO-np/CF Electrodes

	η_{Onset} (V)	LSV η at 1 mA cm^{-2} (V)	electrochemically active Ir sites per gram (mmol $_{Ir}$ g^{-1})	Tafel slope (mV dec^{-1})	$Ir^{III/IV}$ oxidation peak potential (V_{RHE})
Ir	0.20	0.29	0.68	60	0.89
$Ir_{0.92}Cu_{0.08}$	0.20	0.28	0.75	58	0.90
$Ir_{0.89}Cu_{0.11}$	0.19	0.26	0.79	52	0.91
$Ir_{0.86}Cu_{0.14}$	0.19	0.27	0.76	59	0.92
$Ir_{0.80}Cu_{0.20}$	0.20	0.29	0.67	61	0.92
$Ir_{0.66}Cu_{0.34}$	0.20	0.30	0.59	73	0.93

($Ir_{0.89}Ni_{0.11}$) HO-np we reported previously.[18] Figure 1C shows that the selected area diffraction pattern lacks bright rings, which suggests that the sample is a mixture of small crystalline nanoparticles.[23] The measured interplanar spacing is ~0.22 nm, which corresponds to the (200) plane of the IrO_2 structure with tetragonal symmetry (JCPDS No. 86−0330). Similar interplanar spacings are reported for crystallized IrO_2[24,25] and Cu-doped IrO_2.[19] Figure 1D shows the powder X-ray diffraction (XRD) patterns of the washed, isolated $Ir_{0.89}Cu_{0.11}$and Ir HO-np. Both hydrous oxides had common IrO_2 rutile structures with tetragonal symmetry (JCPDS No. 86-0330, space group *P*42/*mnm*). The broad nature of the peaks suggests that the crystalline regions were small.

Figure 2 show the results from the XPS analysis of the Ir, $Ir_{0.89}Cu_{0.11}$, and Cu HO-np. The $4f_{7/2}$ (61.6 eV) and $4f_{5/2}$ (64.5 eV) Ir binding energies in $Ir_{0.89}Cu_{0.11}$, as well as those in Ir ($4f_{7/2}$ (61.9 eV) and $4f_{5/2}$ (64.9 eV)) show that Ir is mainly in the 4^+ oxidation state in both these catalysts (Figure 2A).[26] The 4f binding energies in Ir HO-np also match those reported for IrO_2.[26,27] The Ir-4f peaks in $Ir_{0.89}Cu_{0.11}$ HO-np occur at lower binding energies than Ir HO-np, suggesting that the electron density at Ir is higher in the presence of Cu. Figure 2B shows the XPS spectra of Cu 2p region for the Cu and $Ir_{0.89}Cu_{0.11}$ HO-np. The Cu $2p_{3/2}$ (934.3 eV) and $2p_{1/2}$ (954.1 eV) binding energies were similar, and indicate that Cu is mainly in the 2^+ oxidation state in both.[19,28] Figure S3 shows the deconvoluted Cu $2p_{3/2}$ peak. For Cu HO-np, two deconvoluted peaks at 933.0 and 934.5 eV correspond to Cu(II) oxide and hydroxide.[28] For $Ir_{0.89}Cu_{0.11}$ HO-np, another deconvoluted peak at 935.5 eV is present, which was proposed by Sun et al. to arise from Cu−O−Ir structures in the hydrous oxide.[19] As Ir is mainly in the 4^+ state, and Cu is 2^+, replacing Ir with Cu will reduce the net positive charge from the metals, and may result in oxide vacancies in the HO-np lattice. The decreased net positive charge may also account for the lower binding energies of the Ir-4f peaks in the $Ir_{0.89}Cu_{0.11}$ HO-np. Figure 2C shows the deconvoluted O 1s signal from the Ir HO-np. The deconvolution yielded three peaks with binding energies at ~530.3, 531.4, and 532.8 eV, assigned to lattice oxygen, hydroxyl groups, and absorbed water, respectively.[9,29,30] Figure 2D shows the deconvoluted O 1s signal for $Ir_{0.89}Cu_{0.11}$ HO-np that contains a new peak at 529.5 eV which was not present in Ir or Cu HO-np. This binding energy lies in the middle between the binding energies for Cu−O−Cu (528.8 eV) (Figure S1) and Ir−O−Ir (530.3 eV). We thereby assign this peak to the lattice oxygen atoms bridging Ir and Cu. Strasser et al. observed similar peaks in Ir−Ni oxides, that they assigned to Ir−O−Ni bridging oxides.[9] On the basis of the results of the HRTEM and XPS studies, we propose that the $Ir_{0.89}Cu_{0.11}$ HO-np has a structure similar to IrO_2 with ~11% of the Ir^{4+} atoms replaced by Cu^{2+}. The distribution of Cu atoms is unkown, but the lack of Cu−O−Cu signals, and the uniform shift of the Ir 4f signals suggests that the distribution of Cu is somewhat uniform within the lattice. The uniform replacement of Ir^{4+} by Cu^{2+}, and the larger radius of Cu^{2+} (73 pm) versus Ir^{4+} (63 pm),[31] likely both influence the WOR activity of the catalyst.

Figure 3A shows the voltammetric profiles (1.35−1.55 V_{RHE}, 10 mV s^{-1}) in 0.1 M $HClO_4$ for the $Ir_{1-x}Cu_x$ HO-np series deposited on carbon fiber (CF) paper using Nafion as a binder. The WOR onset potential over $Ir_{0.89}Cu_{0.11}$ HO-np/CF was ~1.42 V_{RHE}, corresponding to ~0.19 V overpotential. The mass activity at 1.48 V_{RHE} reaches 142 A g_{Ir}^{-1}. This activity is higher than other reported IrCu catalysts,[19,20] and it is comparable to $IrNi_{0.125}$ ($Ir_{0.89}Ni_{0.11}$) HO-np, which is among the most active in the literature.[9,16,18,22] Figure 3C shows a plot of the mass activity at 1.48 V_{RHE} of the $Ir_{1-x}Cu_x$ HO-np/CF electrodes against composition. The highest mass activity was obtained with x = 0.11, which was 1.6 times higher than that of Ir HO-np. The catalysts with higher fraction of Cu (x) had lower mass activities.

Figure 3B shows the voltammograms (0.30−1.30 V_{RHE}, 50 mV s^{-1}) of the $Ir_{1-x}Cu_x$ HO-np/CF electrodes. The Ir^{3+}/Ir^{4+} oxidation peaks were centered at ~0.9 V_{RHE} in the anodic scan, and the Ir^{4+}/Ir^{3+} reduction peaks at ~0.87 V_{RHE}. This behavior corresponds to that of IrO_2.[9,18,20,32] Table 2 summarizes the electrochemical parameters obtained for these catalysts. As shown in Table 2, the Ir^{3+}/Ir^{4+} redox peak potential shifts anodically with higher amounts of Cu, indicating that the electron density at Ir^{3+} decreases as the amount of Cu is increased in the lattice.[9] Similar Ir^{3+}/Ir^{4+} peak anodic shifts were observed by Strasser et al. with Ir−Ni mixed oxide electrodes in 0.1 M $HClO_4$.[9] This trend appears to be opposite to the results from the XPS study. We point out that the XPS measurements were of an Ir^{4+}−Cu^{2+} HO-np under vacuum, whereas the LSV results would be influenced to some extent by the interaction between Ir^{3+} and Cu^{2+} within the hydrated HO-np in aqueous acid.

The charge (Q) under the Ir^{3+}/Ir^{4+} oxidation peak was used to estimate the electrochemically active Ir sites. Table 2 lists the moles electrochemically active Ir per gram catalyst calculated based on eq 1.

$$\text{active Ir sites per gram} = \frac{Q(C)}{96485\ (\text{C mol}^{-1}) \times 3.4 \times 10^{-6}\ (g)} \quad (1)$$

The active Ir sites per gram increases by ~16.1% from x = 0 to x = 0.11 and then drops by ~13.2% from x = 0 to x = 0.34. Figure 3D shows the WOR activity (at 0.25 V overpotential) normalized to the moles of active Ir vs the content of Cu (x) in the HO-np. The same trend as the mass activity is observed, with the $Ir_{0.89}Cu_{0.11}$ HO-np/CF electrode being the most active. The accessible Ir site normalized activity of the $Ir_{0.89}Cu_{0.11}$ HO-np was 1.5 times that of Ir HO-np. The mechanism of

DOI: 10.1021/acs.jpcc.6b12164
J. Phys. Chem. C 2017, 121, 5480−5486

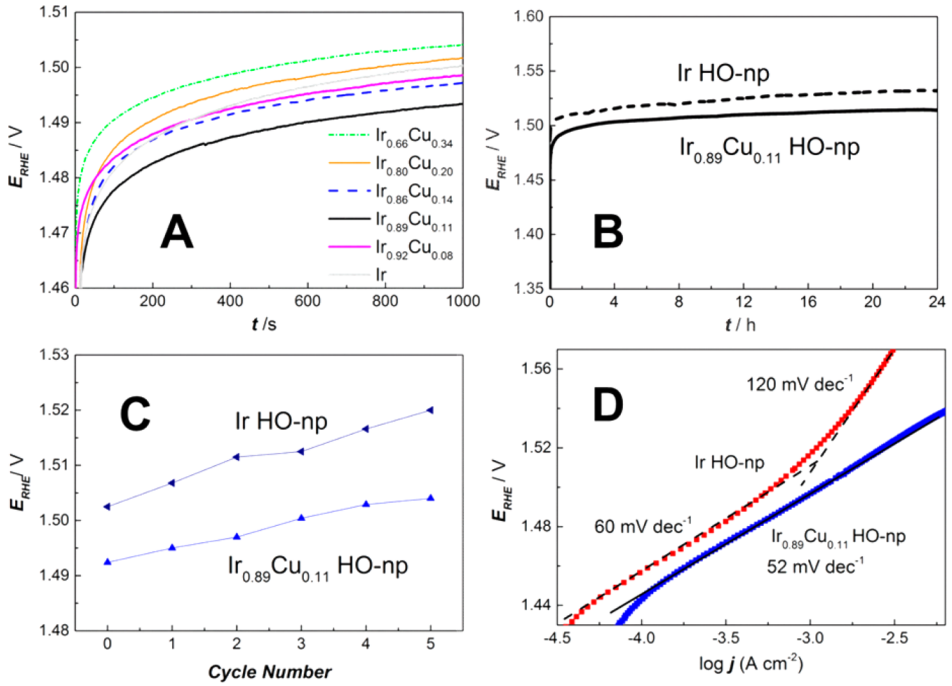

Figure 4. (A) Short-term 1 mA cm^{-2} galvanostatic test on $Ir_{1-x}Cu_x$ HO-np/CF (Ir loading: 17 μg cm^{-2}). (B) 24 h galvanostatic test on $Ir_{0.89}Cu_{0.11}$ and Ir HO-np/CF (Ir loading: 17 μg cm^{-2}). (C) Duty cycle results for $Ir_{0.89}Cu_{0.11}$ and Ir HO-np/CF. (D) Tafel slopes of $Ir_{0.89}Cu_{0.11}$ and Ir HO-np/CF electrodes.

promotion of Ir by Cu is therefore not simply a surface area phenomenon.

Figure 4A shows the results from short-term galvanostatic WOR at 1 mA cm^{-2} with $Ir_{1-x}Cu_x$ HO-np/CF electrodes. The $Ir_{0.89}Cu_{0.11}$ HO-np/CF electrode maintained the set current density at the lowest overpotential among all the catalysts, which leveled out at ~0.26 V (1.49 V_{RHE}) after 1000 s. The 24 h galvanostatic tests were carried out with the $Ir_{0.89}Cu_{0.11}$ and Ir HO-np/CF electrodes (Figure 4B). Both electrodes were quite stable under 1 mA cm^{-2} galvanostatic polarization in acid. The potential for $Ir_{0.89}Cu_{0.11}$ HO-np/CF rose from 1.47 V_{RHE} to 1.50 V_{RHE} within the first 1.5 h, and then leveled out, rising very slowly to 1.51 V_{RHE}, which is ~20 mV lower than the Ir HO-np/CF electrode, and lower than other IrO_x based catalysts in the literature.[16,22] ICP-MS measurements of the electrolyte showed that less than 10% of the Ir or Cu was dissolved during the 24 h galvanostatic oxidation (Table S2).

The duty cycle test developed by Strasser et al. is a good measurement of the stability of the catalysts under close to real electrolyzer conditions.[22] Figure 4C shows the results from duty cycle tests performed with the $Ir_{0.89}Cu_{0.11}$ and Ir HO-np/CF electrodes. After 5 duty cycles, the potential required to reach 1 mA cm^{-2} increased by only 10 mV for the $Ir_{0.89}Cu_{0.11}$ HO-np/CF electrode, while it increased by 18 mV for Ir HO-np/CF. This stability is comparable to the $IrNiO_x$ core–shell particles reported by Strasser et al.[22]

Figure 4D shows the WOR Tafel plots over the $Ir_{0.89}Cu_{0.11}$ and Ir HO-np/CF electrodes. Over Ir HO-np the Tafel slope was ~60 mV dec^{-1} at low overpotentials, and ~120 mV dec^{-1} at high overpotentials. This behavior is well-known for IrO_x catalysts.[33−35] The Tafel slope over $Ir_{0.89}Cu_{0.11}$ HO-np/CF was ~52 mV dec^{-1}, over the range of overpotentials employed for this study. Equations 2−5 show a widely accepted mechanism for the WOR over IrO_x in acid.[34−38]

$$S + H_2O \rightarrow S{-}OH^*_{ads} + H^+ + e^- \quad (2)$$

$$S{-}OH^*_{ads} \rightarrow S{-}OH_{ads} \quad (3)$$

$$S{-}OH_{ads} \rightarrow S{-}O_{ads} + H^+ + e^- \quad (4)$$

$$S{-}O_{ads} + S{-}O_{ads} \rightarrow 2S + O_2 \quad (5)$$

Here S is an active site, and $S{-}OH_{ads}$ is an absorbed hydroxide formed by rearrangement of $S{-}OH^*_{ads}$.[39] This mechanism predicts a Tafel slope ~60 mV dec^{-1} if eq 3 is the turnover-limiting step and eq 2 is a pre-equilibrium electrochemical step. The shift to 120 mV dec^{-1} can be explained by the turnover-limiting step changing to eq 2 at higher overpotentials over Ir HO-np.[22,33,39] The slightly lower Tafel slope over $Ir_{0.89}Cu_{0.11}$ HO-np/CF (~52 vs 60 mV dec^{-1}) suggests that the presence of Cu does not significantly alter the mechanism of WOR, but perhaps changes the relative rates of eqs 2 and 3 to some extent by resulting in oxide vacancies or expanding the oxide lattice. More research is required to investigate the role of Cu in promoting water oxidation activity of Ir HO-np.

■ CONCLUSION

The $Ir_{1-x}Cu_x$ HO-np synthesized with this straightforward, scalable manner are among the most active water oxidation catalysts in acid. The onset overpotential is ~190 mV and the mass activity is over 140 A g_{Ir}^{-1} at 250 mV overpotential with the most active catalyst in the series, $Ir_{0.89}Cu_{0.11}$ HO-np. The $Ir_{0.89}Cu_{0.11}$ HO-np is stable under anodic acidic environment. Preliminary mechanistic investigations showed that the activity enhancement by Cu is not only a surface area effect, and the presence of Cu does not appear to significantly alter the mechanism of the WOR. Research is underway to investigate the mechanism of activation by Cu and to investigate these catalysts in prototype water electrolyzers.

DOI: 10.1021/acs.jpcc.6b12164
J. Phys. Chem. C 2017, 121, 5480−5486

■ ASSOCIATED CONTENT

Supporting Information

The Supporting Information is available free of charge on the ACS Publications website at DOI: 10.1021/acs.jpcc.6b12164.

XPS, ICP-MS, cyclic voltammetry, and Tafel slope plots (PDF)

■ AUTHOR INFORMATION

Corresponding Author

*(S.H.B.) E-mail: sbergens@ualberta.ca.

ORCID

Steven H. Bergens: 0000-0001-7528-8713

Author Contributions

The manuscript was written through contributions of all authors. All authors have given approval to the final version of the manuscript.

Notes

The authors declare no competing financial interest.

■ ACKNOWLEDGMENTS

The authors thank the Natural Sciences and Engineering Research Council of Canada (NSERC), Alberta Ingenuity: Technology Futures, and the University of Alberta for supporting this work. The authors also thank Guangcheng Chen for ICP-MS measurements, Anqiang He for XPS measurements, and Glynis de Silveira for HR-TEM analysis.

■ REFERENCES

(1) Hosseini, S. E.; Wahid, M. A. Hydrogen Production From Renewable and Sustainable Energy Resources: Promising Green Energy Carrier for Clean Development. *Renewable Sustainable Energy Rev.* **2016**, *57*, 850−866.

(2) Liu, J.; Liu, Y.; Liu, N.; Han, Y.; Zhang, X.; Huang, H.; Lifshitz, Y.; Lee, S.-T.; Zhong, J.; Kang, Z. Metal-Free Efficient Photocatalyst for Stable Visible Water Splitting via a Two-Electron Pathway. *Science* **2015**, *347*, 970−974.

(3) Turner, J. A. Sustainable Hydrogen Production. *Science* **2004**, *305*, 972−974.

(4) Dincer, I.; Acar, C. Review and Evaluation of Hydrogen Production Methods for Better Sustainability. *Int. J. Hydrogen Energy* **2015**, *40*, 11094−11111.

(5) Song, F.; Hu, X. Exfoliation of Layered Double Hydroxides for Enhanced Oxygen Evolution Catalysis. *Nat. Commun.* **2014**, *5*, 4477.

(6) Carmo, M.; Fritz, D. L.; Mergel, J.; Stolten, D. A Comprehensive Review on PEM Water Electrolysis. *Int. J. Hydrogen Energy* **2013**, *38*, 4901−4934.

(7) Fabbri, E.; Habereder, A.; Waltar, K.; Kotz, R.; Schmidt, T. J. Developments and Perspectives of Oxide-Based Catalysts for the Oxygen Evolution Reaction. *Catal. Sci. Technol.* **2014**, *4*, 3800−3821.

(8) Abdol Rahim, A. H.; Tijani, A. S.; Kamarudin, S. K.; Hanapi, S. An Overview of Polymer Electrolyte Membrane Electrolyzer for Hydrogen Production: Modeling and Mass Transport. *J. Power Sources* **2016**, *309*, 56−65.

(9) Reier, T.; Pawolek, Z.; Cherevko, S.; Bruns, M.; Jones, T.; Teschner, D.; Selve, S.; Bergmann, A.; Nong, H. N.; Schlögl, R.; et al. Molecular Insight in Structure and Activity of Highly Efficient, Low-Ir Ir−Ni Oxide Catalysts for Electrochemical Water Splitting (OER). *J. Am. Chem. Soc.* **2015**, *137*, 13031−13040.

(10) Katsounaros, I.; Cherevko, S.; Zeradjanin, A. R.; Mayrhofer, K. J. J. Oxygen Electrochemistry as a Cornerstone for Sustainable Energy Conversion. *Angew. Chem., Int. Ed.* **2014**, *53*, 102−121.

(11) Danilovic, N.; Subbaraman, R.; Chang, K.-C.; Chang, S. H.; Kang, Y. J.; Snyder, J.; Paulikas, A. P.; Strmcnik, D.; Kim, Y.-T.; Myers, D.; et al. Activity−Stability Trends for the Oxygen Evolution Reaction on Monometallic Oxides in Acidic Environments. *J. Phys. Chem. Lett.* **2014**, *5*, 2474−2478.

(12) Danilovic, N.; Subbaraman, R.; Chang, K. C.; Chang, S. H.; Kang, Y.; Snyder, J.; Paulikas, A. P.; Strmcnik, D.; Kim, Y. T.; Myers, D.; et al. Using Surface Segregation To Design Stable Ru-Ir Oxides for the Oxygen Evolution Reaction in Acidic Environments. *Angew. Chem., Int. Ed.* **2014**, *53*, 14016−14021.

(13) Lettenmeier, P.; Wang, L.; Golla-Schindler, U.; Gazdzicki, P.; Cañas, N. A.; Handl, M.; Hiesgen, R.; Hosseiny, S. S.; Gago, A. S.; Friedrich, K. A. Nanosized IrO_x−Ir Catalyst with Relevant Activity for Anodes of Proton Exchange Membrane Electrolysis Produced by a Cost-Effective Procedure. *Angew. Chem.* **2016**, *128*, 752−756.

(14) Lee, B.-S.; Ahn, S. H.; Park, H.-Y.; Choi, I.; Yoo, S. J.; Kim, H.-J.; Henkensmeier, D.; Kim, J. Y.; Park, S.; Nam, S. W.; et al. Development of Electrodeposited IrO_2 Electrodes as Anodes in Polymer Electrolyte Membrane Water Electrolysis. *Appl. Catal., B* **2015**, *179*, 285−291.

(15) Smith, R. D. L.; Sporinova, B.; Fagan, R. D.; Trudel, S.; Berlinguette, C. P. Facile Photochemical Preparation of Amorphous Iridium Oxide Films for Water Oxidation Catalysis. *Chem. Mater.* **2014**, *26*, 1654−1659.

(16) Nong, H. N.; Gan, L.; Willinger, E.; Teschner, D.; Strasser, P. IrO_x Core-Shell Nanocatalysts for Cost- and Energy-Efficient Electrochemical Water Splitting. *Chem. Sci.* **2014**, *5*, 2955−2963.

(17) Cherevko, S.; Geiger, S.; Kasian, O.; Kulyk, N.; Grote, J.-P.; Savan, A.; Shrestha, B. R.; Merzlikin, S.; Breitbach, B.; Ludwig, A.; et al. Oxygen and Hydrogen Evolution Reactions on Ru, RuO_2, Ir, and IrO_2 Thin Film Electrodes in Acidic and Alkaline Electrolytes: A Comparative Study on Activity and Stability. *Catal. Today* **2016**, *262*, 170−180.

(18) Moghaddam, R. B.; Wang, C.; Sorge, J. B.; Brett, M. J.; Bergens, S. H. Easily Prepared, High Activity Ir−Ni Oxide Catalysts for Water Oxidation. *Electrochem. Commun.* **2015**, *60*, 109−112.

(19) Sun, W.; Song, Y.; Gong, X.-Q.; Cao, L.-m.; Yang, J. An Efficiently Tuned d-Orbital Occupation of IrO_2 by Doping with Cu for Enhancing the Oxygen Evolution Reaction Activity. *Chem. Sci.* **2015**, *6*, 4993−4999.

(20) Wang, C.; Sui, Y.; Xiao, G.; Yang, X.; Wei, Y.; Zou, G.; Zou, B. Synthesis of Cu-Ir Nanocages with Enhanced Electrocatalytic Activity for the Oxygen Evolution Reaction. *J. Mater. Chem. A* **2015**, *3*, 19669−19673.

(21) Hu, W.; Zhong, H.; Liang, W.; Chen, S. Ir-Surface Enriched Porous Ir−Co Oxide Hierarchical Architecture for High Performance Water Oxidation in Acidic Media. *ACS Appl. Mater. Interfaces* **2014**, *6*, 12729−12736.

(22) Nong, H. N.; Oh, H.-S.; Reier, T.; Willinger, E.; Willinger, M.-G.; Petkov, V.; Teschner, D.; Strasser, P. Oxide-Supported $IrNiO_x$ Core−Shell Particles as Efficient, Cost-Effective, and Stable Catalysts for Electrochemical Water Splitting. *Angew. Chem., Int. Ed.* **2015**, *54*, 2975−2979.

(23) Qiu, Y.; Xin, L.; Li, W. Electrocatalytic Oxygen Evolution over Supported Small Amorphous Ni−Fe Nanoparticles in Alkaline Electrolyte. *Langmuir* **2014**, *30*, 7893−7901.

(24) Ryu, W.-H.; Lee, Y. W.; Nam, Y. S.; Youn, D.-Y.; Park, C. B.; Kim, I.-D. Crystalline IrO_2-Decorated TiO_2 Nanofiber Scaffolds For Robust and Sustainable Solar Water Oxidation. *J. Mater. Chem. A* **2014**, *2*, 5610−5615.

(25) Li, Y.; Yu, Z.; Meng, J.; Li, Y. Enhancing the Activity of a SiC−TiO_2 Composite Catalyst for Photo-Stimulated Catalytic Water Splitting. *Int. J. Hydrogen Energy* **2013**, *38*, 3898−3904.

(26) Fóti, G.; Mousty, C.; Reid, V.; Comninellis, C. Characterization of DSA Type Electrodes Prepared by Rapid Thermal Decomposition of the Metal Precursor. *Electrochim. Acta* **1998**, *44*, 813−818.

(27) Kötz, R.; Neff, H.; Stucki, S. Anodic Iridium Oxide Films: XPS-Studies of Oxidation State Changes and. *J. Electrochem. Soc.* **1984**, *131*, 72−77.

(28) Du, J.; Chen, Z.; Ye, S.; Wiley, B. J.; Meyer, T. J. Copper as a Robust and Transparent Electrocatalyst for Water Oxidation. *Angew. Chem., Int. Ed.* **2015**, *54*, 2073−2078.

DOI: 10.1021/acs.jpcc.6b12164
J. Phys. Chem. C 2017, 121, 5480−5486

(29) Dupin, J.-C.; Gonbeau, D.; Vinatier, P.; Levasseur, A. Systematic XPS Studies of Metal Oxides, Hydroxides and Peroxides. *Phys. Chem. Chem. Phys.* **2000**, *2*, 1319−1324.
(30) Grosvenor, A. P.; Kobe, B. A.; McIntyre, N. S. Studies of the Oxidation of Iron by Water Vapour Using X-Ray Photoelectron Spectroscopy and QUASES. *Surf. Sci.* **2004**, *572*, 217−227.
(31) Shannon, R. Revised Effective Ionic Radii and Systematic Studies of Interatomic Distances in Halides and Chalcogenides. *Acta Crystallogr., Sect. A: Cryst. Phys., Diffr., Theor. Gen. Crystallogr.* **1976**, *32*, 751−767.
(32) Conway, B. E.; Mozota, J. Surface and Bulk Processes at Oxidized Iridium Electrodes—II. Conductivity-Switched Behaviour of Thick Oxide Films. *Electrochim. Acta* **1983**, *28*, 9−16.
(33) Lyons, M. E. G.; Floquet, S. Mechanism of Oxygen Reactions at Porous Oxide Electrodes. Part 2-Oxygen Evolution at RuO_2, IrO_2 and $Ir_xRu_{1-x}O_2$ Electrodes in Aqueous Acid and Alkaline Solution. *Phys. Chem. Chem. Phys.* **2011**, *13*, 5314−5335.
(34) Da Silva, L. A.; Alves, V. A.; Trasatti, S.; Boodts, J. F. C. Surface and Electrocatalytic Properties of Ternary Oxides $Ir_{0.3}Ti_{(0.7-x)}Pt_xO_2$. Oxygen Evolution from Acidic Solution. *J. Electroanal. Chem.* **1997**, *427*, 97−104.
(35) Hu, J.-M.; Zhang, J.-Q.; Cao, C.-N. Oxygen Evolution Reaction on IrO_2-Based DSA® Type Electrodes: Kinetics Analysis of Tafel Lines and EIS. *Int. J. Hydrogen Energy* **2004**, *29*, 791−797.
(36) Zhao, Y.; Vargas-Barbosa, N. M.; Hernandez-Pagan, E. A.; Mallouk, T. E. Anodic Deposition of Colloidal Iridium Oxide Thin Films from Hexahydroxyiridate(IV) Solutions. *Small* **2011**, *7*, 2087−2093.
(37) Da Silva, L. A.; Alves, V. A.; Da Silva, M. A. P.; Trasatti, S.; Boodts, J. F. C. Morphological, Chemical, and Electrochemical Properties of Ti/(TiO_2+IrO_2) Electrodes. *Can. J. Chem.* **1997**, *75*, 1483−1493.
(38) Reier, T.; Nong, H. N.; Teschner, D.; Schlögl, R.; Strasser, P. Electrocatalytic Oxygen Evolution Reaction in Acidic Environments − Reaction Mechanisms and Catalysts. *Adv. Energy Mater.* **2017**, *7*, 1601275.
(39) De Faria, L. A.; Boodts, J. F. C.; Trasatti, S. Electrocatalytic Properties of Ternary Oxide Mixtures of Composition $Ru_{0.3}Ti_{(0.7-x)}Ce_xO_2$: Oxygen Evolution from Acidic Solution. *J. Appl. Electrochem.* **1996**, *26*, 1195−1199.

DOI: 10.1021/acs.jpcc.6b12164
J. Phys. Chem. C 2017, 121, 5480−5486